

Defective by design: Vanadium-substituted iron oxide nanoarchitectures as cation-insertion hosts for electrochemical charge storage

Christopher N. Chervin,^{*a} Jesse S. Ko,^b Bryan W. Miller,^a Lisa Dudek,^c Azzam N. Mansour,^d Martin D. Donakowski,^a Todd Brintlinger,^e Pavel Gogotsi,^a Soma Chattopadhyay,^{f,g} Tomohiro Shibata,^g Joseph F. Parker,^a Benjamin P. Hahn,^a Debra R. Rolison,^a and Jeffrey W. Long^{*a}

^a U. S. Naval Research Laboratory, Surface Chemistry Branch (Code 6170), Washington, D.C. 20375, USA

^b Department of Materials Science and Engineering, University of California at Los Angeles (UCLA), Los Angeles, California 90095, USA

^c Department of Chemistry and Biochemistry, University of California at Los Angeles (UCLA), Los Angeles, California 90095, USA

^d Naval Surface Warfare Center, Carderock Division, Materials and Power Systems Branch (Code 6160), West Bethesda, MD, 20817, USA

^e U. S. Naval Research Laboratory, Materials and Sensors Branch (Code 6360), Washington, D.C. 20375, USA

^f Physical Sciences Department, Elgin Community College, 1700 Spartan Drive, Elgin, IL 60123.

^g Previously at: Sector 10 ID, CSRRRI- IIT, Advanced Photon Source, 9700 S . Cass Avenue, Lemont, IL 60439.

*Corresponding authors: christopher.chervin@nrl.navy.mil (C. N. Chervin); jeffrey.long@nrl.navy.mil (J. W. Long)

Figure S1

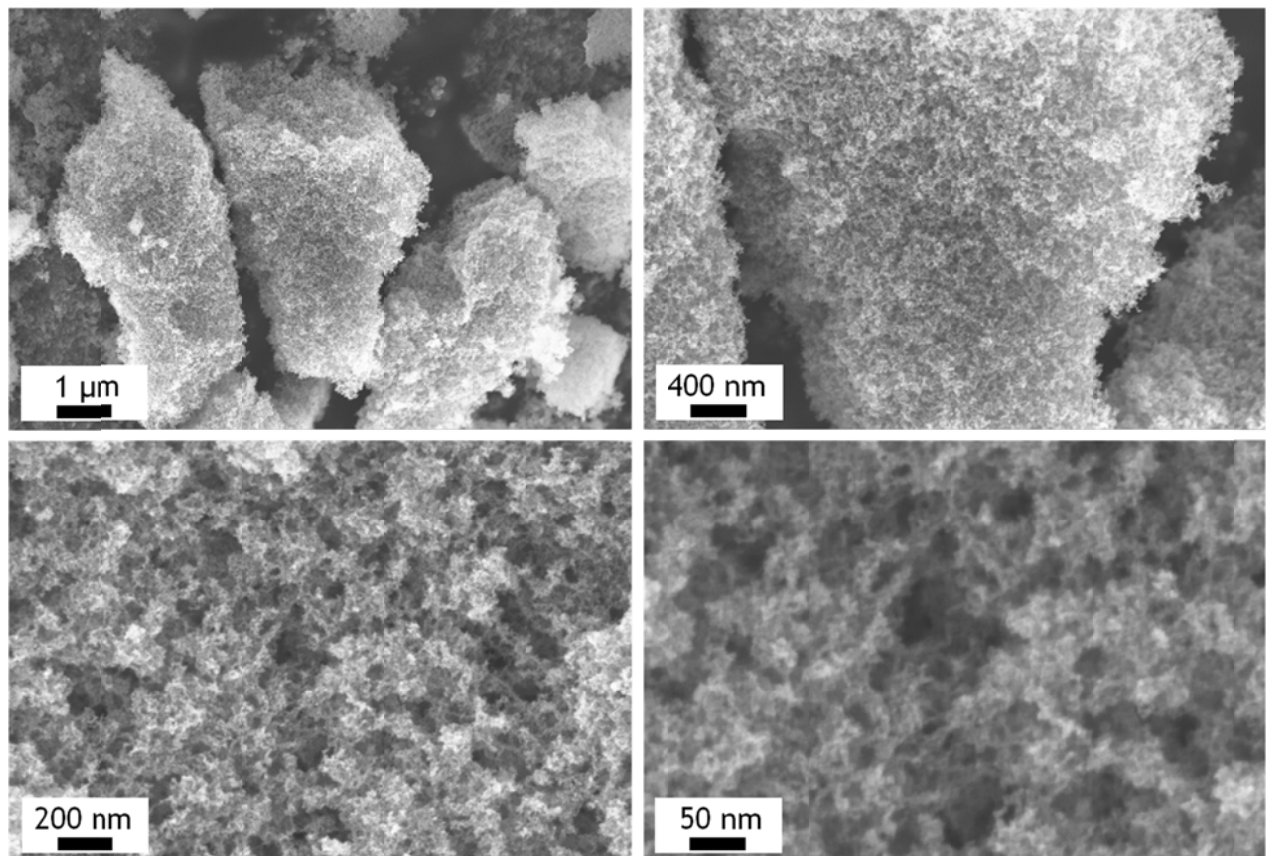


Fig S1 Scanning electron micrographs of an as-synthesized VFe_2O_x aerogel at different magnifications. The low-magnification images (upper) demonstrate that the through-connected porosity permeates across the large length-scales of aggregates that remain after pulverizing the aerogel monolith. The high-magnification images (lower) show the connected, tendril-like solid-network that connects the nanometric oxide particles comprising the aerogel.

Figure S2

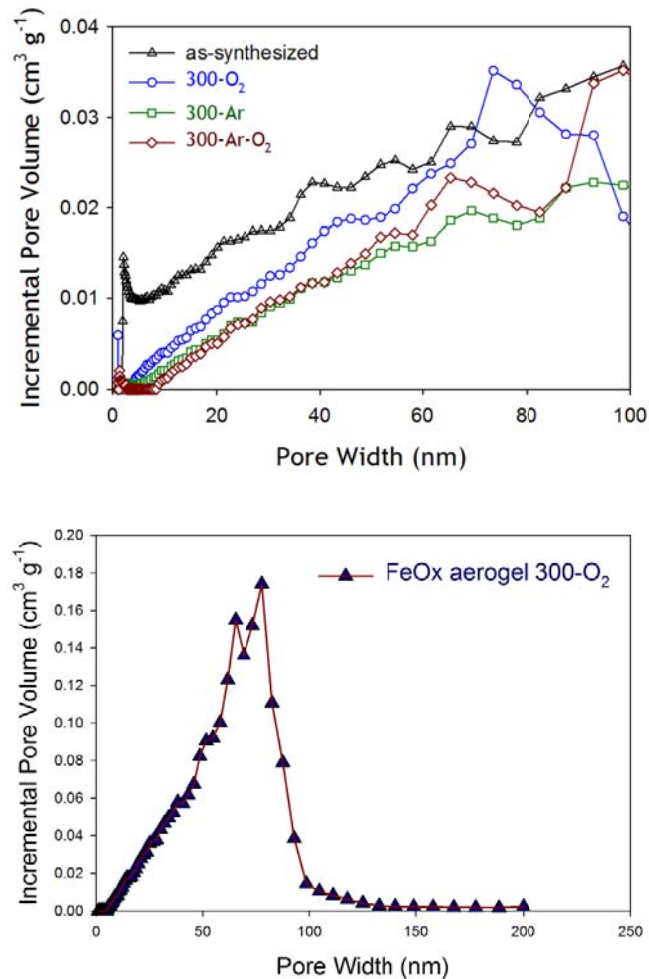


Fig S2 Pore size distribution plots derived from N₂-sorption porosimetry for (top) VFe₂O_x aerogels and (bottom) a 300-O₂ FeO_x aerogel.

Figure S3

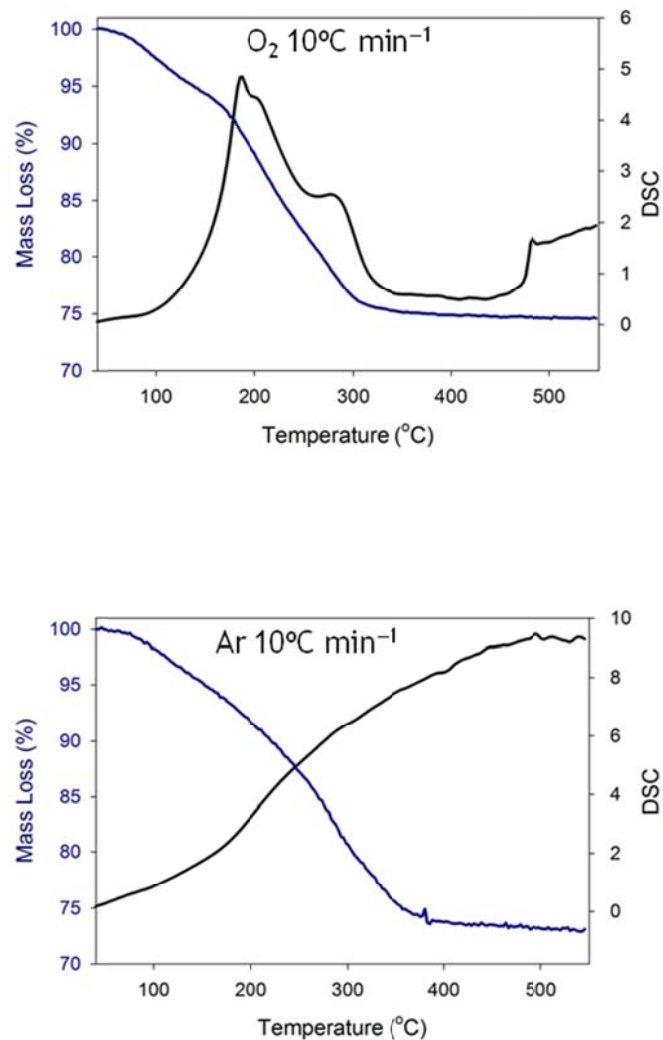


Fig S3 Thermogravimetric analysis and differential scanning calorimetry of as-synthesized VFe_2O_x aerogels at $10^\circ\text{C min}^{-1}$ under flowing: O_2 (top) and Ar (bottom).

Figure S4

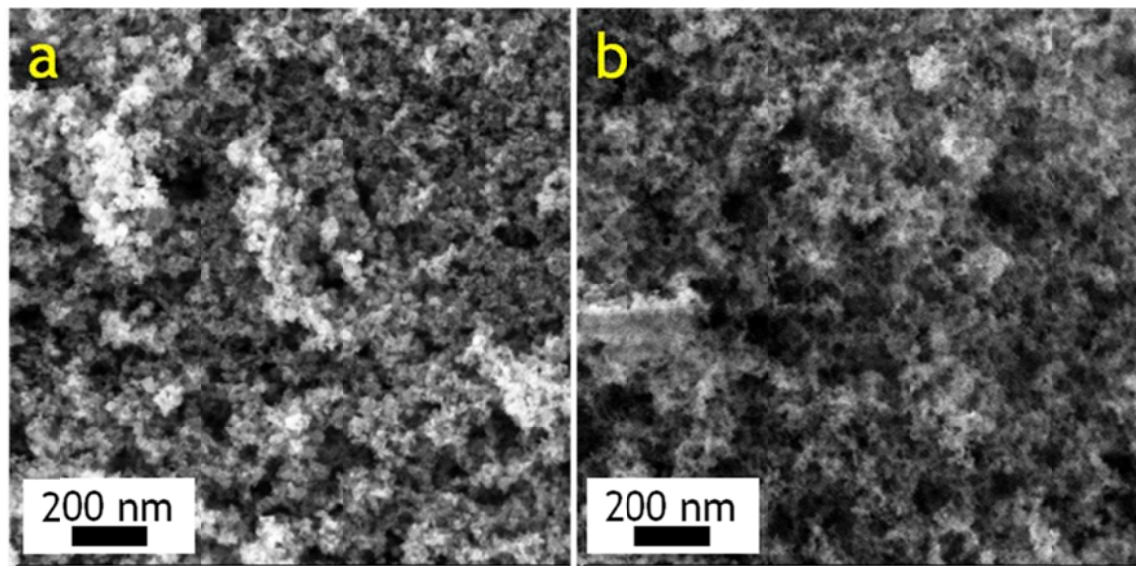


Fig S4 Scanning electron micrographs of VFe₂O_x aerogels: (a) 300-Ar, and (b) 300-Ar-O₂.

Figure S5

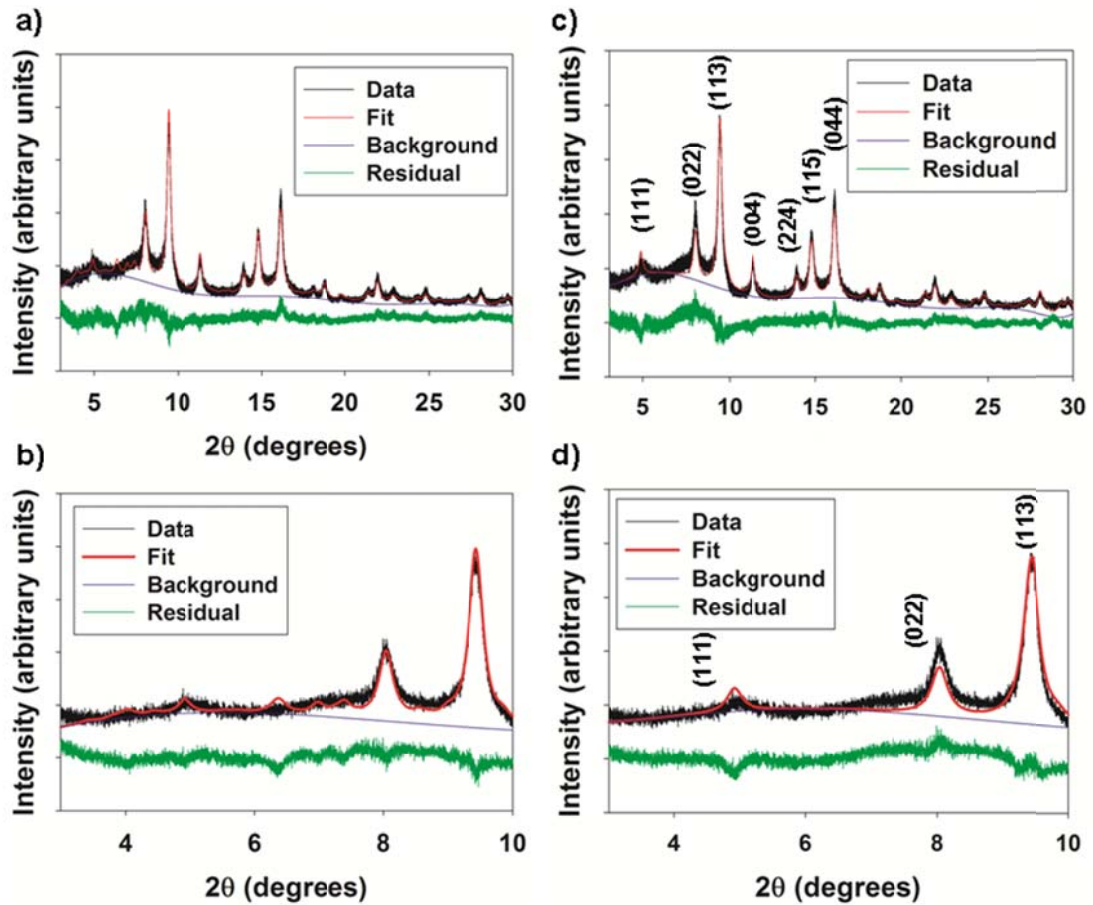


Fig S5 Rietveld fit of synchrotron powder X-ray diffraction data (PXRD) for a 300-Ar VFe₂O_x aerogel. ($\lambda = 0.413851 \text{ \AA}$). a) Fit of 300-Ar with a maghemite structure (spacegroup $P4_332$) from 3–30°, b) Fit of 300-Ar with a maghemite structure shown from 3–10°, c) fit of 300-Ar with a magnetite structure (spacegroup $Fd\text{-}3m$) from 3–30°, d) Fit of 300-Ar with a magnetite structure shown from 3–10°. The fits at low 2θ with a maghemite structure show peaks that are not present in the data – the (nano)crystalline phase thus more correctly fits to the magnetite structure.

Figure S6

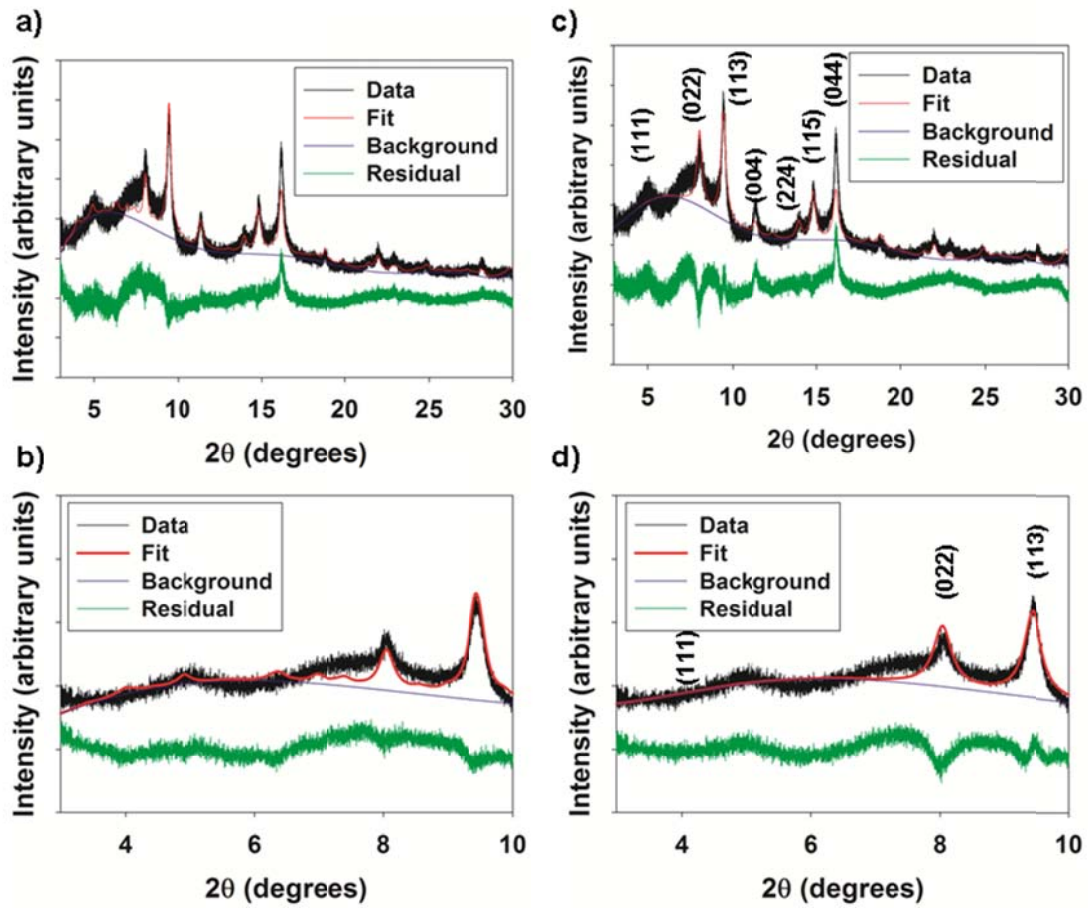


Fig S6 Rietveld fit of synchrotron powder X-ray diffraction data (PXRD) for a 300-Ar-O₂ VFe₂O_x aerogel ($\lambda = 0.413851 \text{ \AA}$) a) Fit of 300-Ar-O₂ with a maghemite structure (spacegroup $P4_332$) from 3 – 30°, b) Fit of 300-Ar-O₂ with a maghemite structure shown from 3–10°, c) fit of 300-Ar-O₂ with a magnetite structure (spacegroup $Fd\text{-}3m$) from 3–30°, d) Fit of 300-Ar-O₂ with a magnetite structure shown from 3–10°. The fits at low 2θ with a maghemite structure show peaks that are not present in the data – the (nano)crystalline phase thus more correctly fits to the magnetite structure.

Figure S7

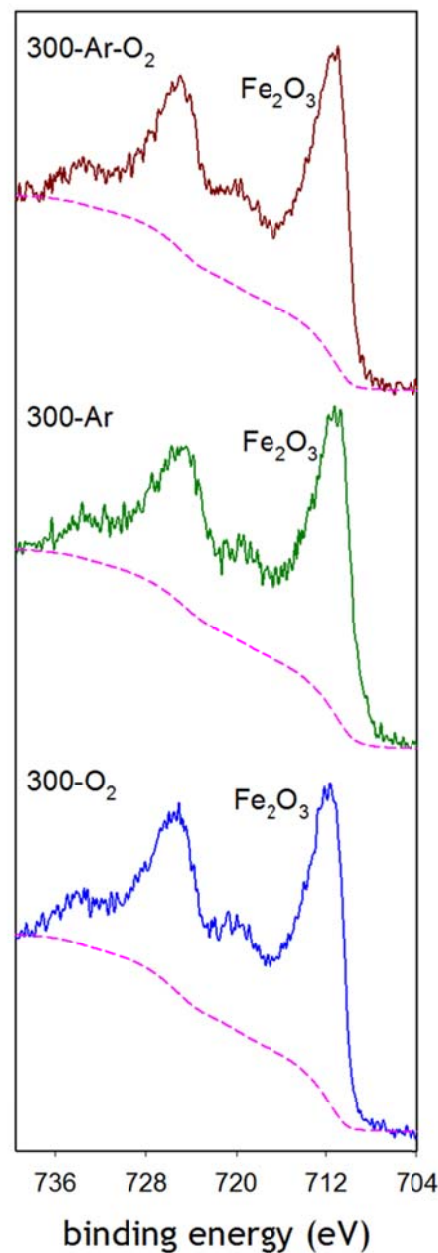


Fig S7 X-ray photoelectron spectra of the Fe2p_{1/2} binding energy for VFe₂O_x aerogels: 300-O₂ (—), 300-Ar (—), 300-Ar-O₂ (—), and background fit (— —).

Figure S8

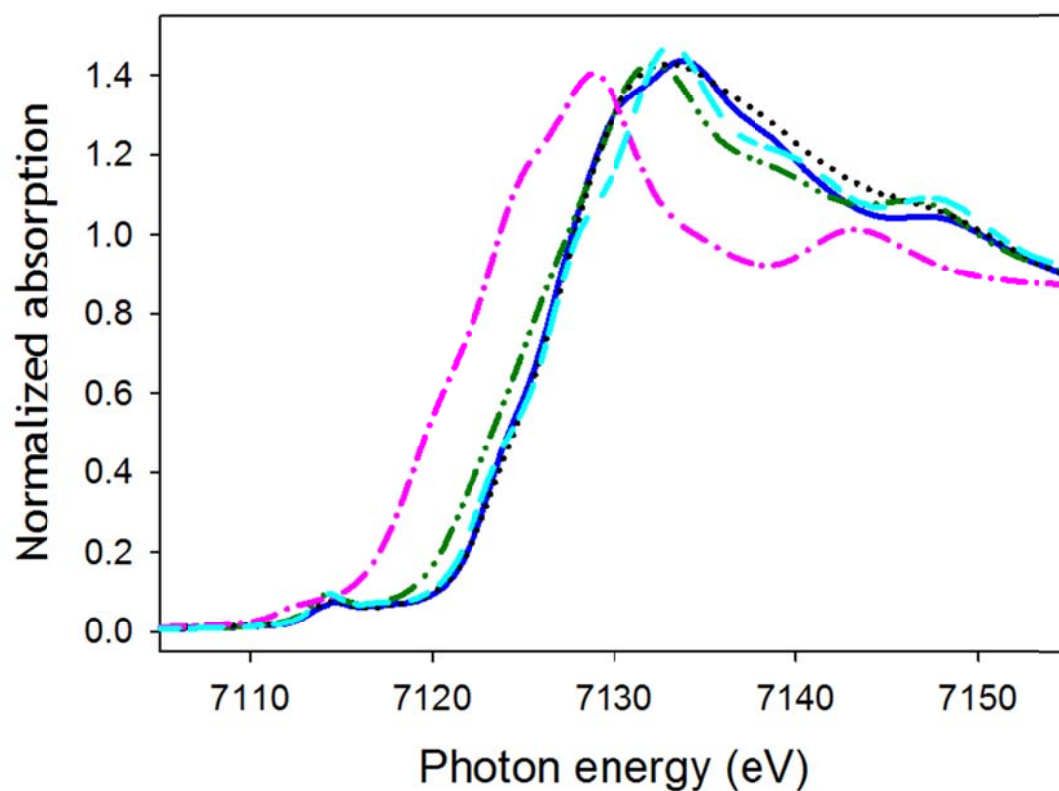


Fig S8 Fe K-edge XANES for FeOx aerogels: 300-O₂ (—), 300-Ar (—•—), and as-synthesized (••); and iron oxide standards: FeO (—•—) and Fe₂O₃ (——).

Figure S9

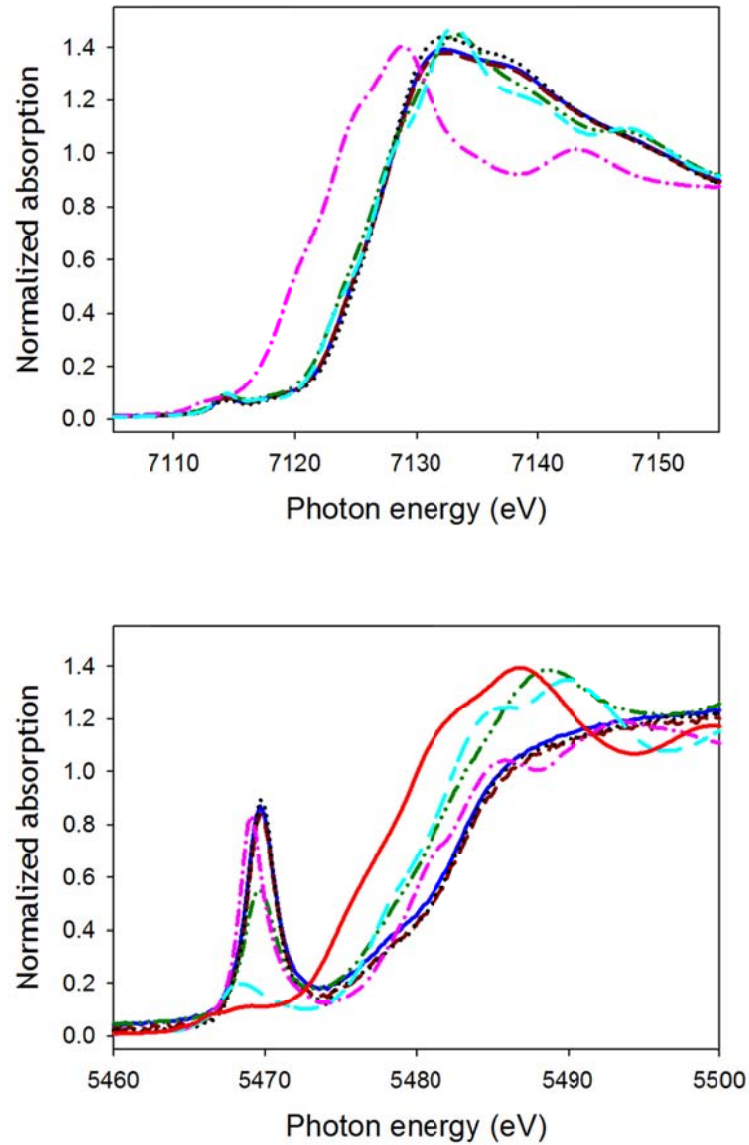


Fig S9 Fe (top) and V (bottom) K-edge XANES for VFe₂O_x aerogels: 300-O₂ (—), 300-Ar-O₂ (---), 300-Ar (-•-), and as-synthesized (•••). Iron oxide standards (top): FeO (-•-) and Fe₂O₃ (—); vanadium oxide standards (bottom): V₂O₅ (-•-) and VO₂ (—), and V₂O₃ (—).

Figure S10

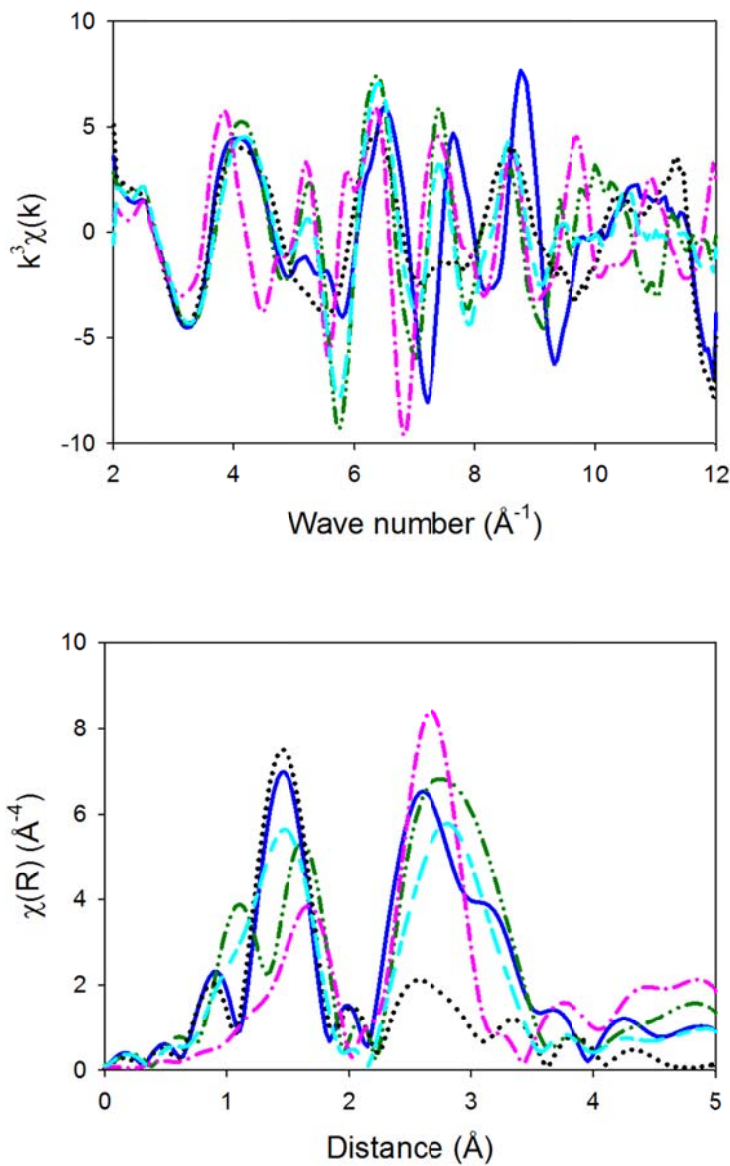


Fig S10 Fe K-edge EXAFS spectra (top) and Fourier transform of EXAFS spectra (bottom) for FeOx aerogels: 300-O₂ (—), 300-Ar (---) and as-synthesized (•••). Iron oxide standards: FeO (-•-) and Fe₂O₃ (—).

Figure S11

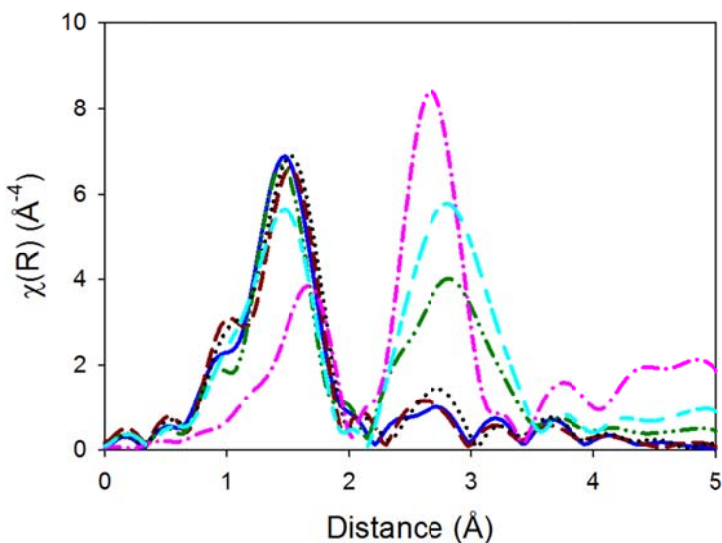
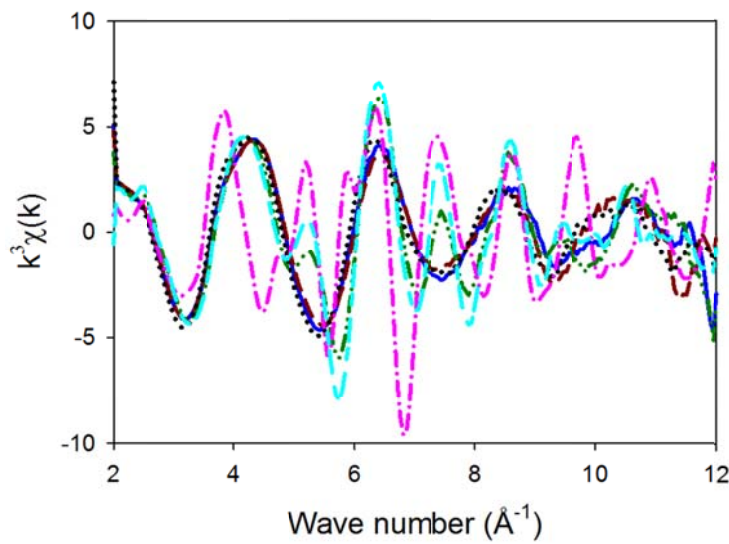


Fig S11 Fe K-edge EXAFS spectra (top) and Fourier transform of EXAFS spectra (bottom) for VFe₂O_x aerogels: 300-O₂ (—), 300-Ar-O₂ (---), 300-Ar (•—), and as-synthesized (•••). Iron oxide standards: FeO (—•—) and Fe₂O₃ (——).

Figure S12

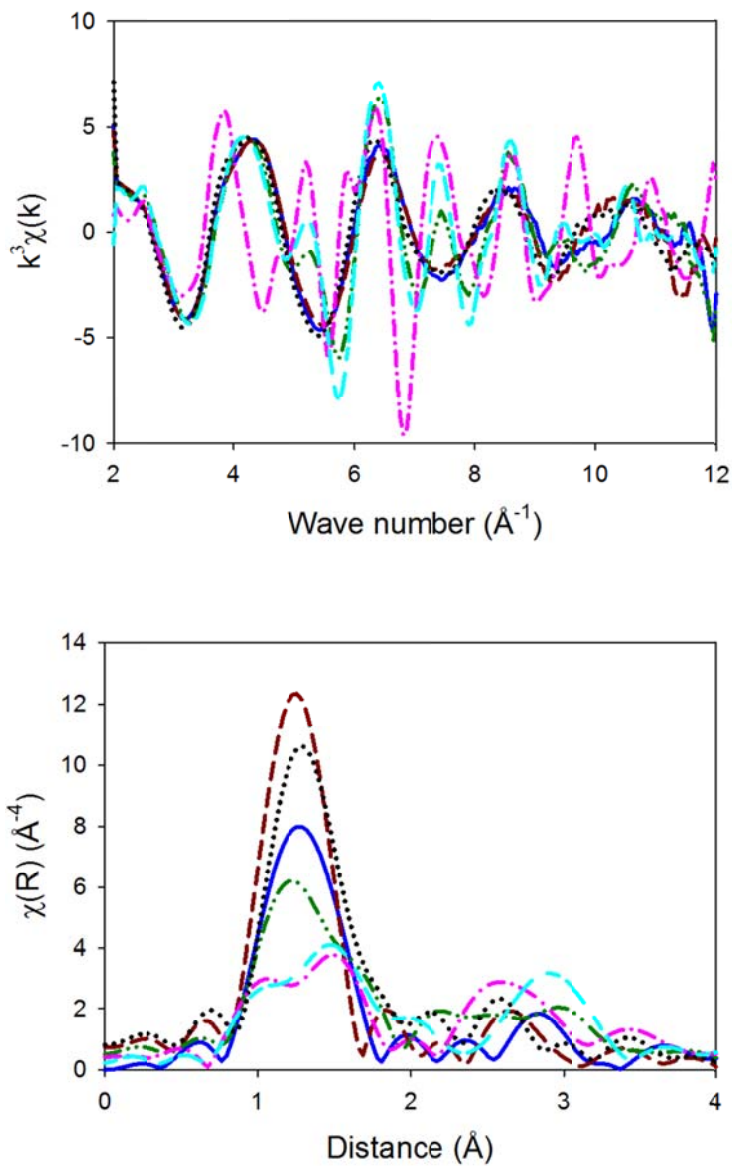


Fig S12 V K-edge EXAFS spectra (top) and Fourier transform of EXAFS spectra (bottom) for VFe₂O_x aerogels: 300-O₂ (—), 300-Ar-O₂ (— — —), 300-Ar (—•—), and as-synthesized (•••). Vanadium oxide standards: V₂O₅ (—•—) and VO₂ (— —).